Mineralogical Characteristics and Color Genesis of Zibai Jade

Linhui Song , Mingyue He * , Ziyun Zhang , Ling Yang

Posted Date: 18 September 2025

doi: 10.20944/preprints202509.1587.v1

Keywords: hydrogrossular; mineral characteristics; chromogenic mechanism; formation mechanism

 doi:10.20944/preprints202509.1587.v1

Article

Mineralogical Characteristics and Color Genesis of Zibai Jade

Linhui Song, Mingyue He *, Ziyun Zhang and Ling Yang

School of Gemmology, China University of Geosciences, Beijing 10083, China

* Correspondence: hemy@cugb.edu.cn

Abstract

Zibai Jade is a recently identified hydrogrossular-dominant jade originating from Shaanxi Province, China. It constitutes a polymineralic aggregate composed predominantly of hydrogrossular, with minor proportions of vesuvianite, diopside, chlorite, uvarovite, and calcite. A multi-method analytical approach was employed to characterize the jade, incorporating conventional gemological testing, polarizing microscopy, SEM, XRD, BSE, XRF, EPMA, as well as UV-Vis, infrared IR. These techniques enabled a detailed examination of its mineralogy, surface features, and color origin. The stone displays heterogeneous color distribution, featuring a base hue of light green to yellowish-green, accompanied by distinct occurrences of emerald-green spots, dark green spots, mossy green inclusions, white patches, white veinlets, and black dot with a green ring.Microanalytical results indicate that the emerald-green spots are principally composed of uvarovite. The dark green sports are dominated by hydrogrossular, diopside, and chlorite. Fibrous green inclusions consist mainly of chlorite and Cr-bearing grossular. White patches and veinlets are primarily composed of calcite. The black dot with a green ring are predominantly comprised of chromite and uvarovite.Coloration is attributed to the combined influence of Fe and Cr^{3+}. The formation of the jade involved three mineralization stages: protolith accumulation, high-temperature metasomatism, and retrograde alteration. The interplay of these processes resulted in the development of Zibai Jade, which exhibits a dense texture and attractive coloration.

Keywords: hydrogrossular; mineral characteristics; chromogenic mechanism; formation mechanism

1. Introduction

Zibai Jade is a mineral aggregate primarily composed of hydrogrossular, with minor amounts of vesuvianite, diopside, uvarovite, calcite, and chlorite, exhibiting a cryptocrystalline texture15 [1]. It exhibits a diverse color range, including colorless, green, pink, brown, and yellow hues. The most desirable variety is an emerald-like green, closely resembling jadeite. It was first discovered in Tsavo National Park, Kenya, hence it is also known as tsavorite [2]. Subsequent discoveries have been reported in various localities, including South Africa, Myanmar, the United States, New Zealand, and Qinghai Province of China.

Due to its fine texture and diverse coloration, hydrogrossular jade has attracted considerable attention from both researchers and gemological institutions. In 2023, Yalong Zheng from the China University of Geosciences (Wuhan) conducted a series of experimental analyses on pink hydrogrossular jade. The results confirmed that its mineral composition is primarily hydrogrossular and vesuvianite, and its pink coloration is mainly attributed to trace amounts of Mn^{2+} within the hydrogrossular component [3]. In 2021, a study conducted by the Gem and Jewelry Institute of Thailand (GIT) Gem Testing Laboratory—Thailand's national gemological research center—utilized infrared and Raman spectroscopy to investigate light yellow and tan hydrogrossular jade. The research successfully identified the characteristic spectral features of brownish-yellow varieties of hydrogrossular jade [4] In 2015, gemological examination and analysis conducted by Lai-Tai-An Gem Laboratory—a professional gemological institution in Taiwan, China—on two green jadeite-imitation

 doi:10.20944/preprints202509.1587.v1

bracelets, identified them as hydrogrossular jade through conventional gemological testing and spectroscopic methods [5]. In 2014, Yanran Xu from the China University of Geosciences, Beijing, clarified the mineral composition and spectroscopic characteristics of hydrogrossular jade from the Tawmaw mining district in Myanmar through a series of systematic investigations [6]. In 2011, gemological analysis performed at the GIA New York Laboratory utilized infrared and Raman spectroscopy to examine three similar green jade samples. The results confirmed one of them to be hydrogrossular jade [7].

In recent years, hydrogrossular-dominant jade was discovered in Liuba County, Shaanxi Province, China. It is locally named "Zibai Jade" after the renowned Zibai Mountain—dubbed the "foremost mountain" along the ancient Qinba Thousand-Li Plank Road—which is also located within the county. The jade is predominantly characterized by yellow and green tones. Previous studies have documented vesuvianite jade from this region [8]; however, the hydrogrossular variety has not been reported. This study selects four specimens collected from the mining area and employs a series of tests to clarify the mineralogical characteristics and chromogenic mechanism of Zibai Jade, while providing a preliminary analysis of its formation mechanism.

2. Materials and Methods

Zibai Jade is primarily sourced from the Shimawan area in Liuba County, Hanzhong, Shaanxi Province. This region is situated on the northwestern margin of the South Qinling Orogenic Belt, near the southern boundary of the Late Neo-Proterozoic to Early Paleozoic Shangdan Suture Zone and the northern edge of the Late Triassic Mianlue Suture Zone [9,10]. The strata exposed in this region predominantly belong to the Silurian and Devonian systems, with lithologies mainly consisting of carbonate rocks, quartz sandstone, and limestone [11]. Magmatic rocks in the area are predominantly composed of Indosinian granodiorite [12]. The jade occurs as stratiform and massive bodies within the contact zone between igneous rocks and carbonate formations. It is commonly associated with a vesuvianite-dominated jade variety in the same locality. A gradational contact is observed between the jade and its host rocks. Grayish-white to white calcite, occurring as irregular veinlets, extends from the proximal host rocks into the jade material. Four representative samples of Zibai Jade (designated ZB-1 to ZB-4; Figure 1), exhibiting distinct color characteristics, were selected for detailed gemological and mineralogical analysis, with a particular focus on their coloration mechanisms.

After being polished and prepared as thin sections, the samples underwent conventional gemological testing at the National Infrastructure of Mineral, Rock, and Fossil Resources for Science and Technology (NIMRF). The properties measured included refractive index, specific gravity, ultraviolet fluorescence, and Chelsea filter response [13].

X-ray diffraction (XRD) analysis was conducted using a Rigaku SmartLab (9 kW) X-ray powder diffractometer at the X-ray Laboratory of the China University of Geosciences, Beijing (CUGB), under standard analytical conditions. The instrument was equipped with a conventional copper-target X-ray tube (operating at 40 kV and 200 mA) and a graphite monochromator. The analysis was performed in continuous scanning mode with a step size of 0.02° and a scanning speed of 4°/min. The sample was ground into 300-mesh powder and stored immediately to minimize contamination and oxidation.The experimental data were normalized and subsequently analyzed using MDI Jade 6.5 software. The obtained diffraction patterns were compared with reference patterns from the JCPDS database using PDF cards for standard mineral identification.

Surface morphology and backscattered electron (BSE) imaging of the samples were conducted using a Phenom XL desktop scanning electron microscope at the National Infrastructure of Mineral, Rock, and Fossil Resources for Science and Technology (NIMRF).The analyses were performed under an accelerating voltage of 15 kV and at magnifications ranging from 1,500× to 27,500×. Backscattered electron (BSE) imaging was performed on polished sections and probe slices prepared from the samples, which were carbon-coated before analysis.

 doi:10.20944/preprints202509.1587.v1

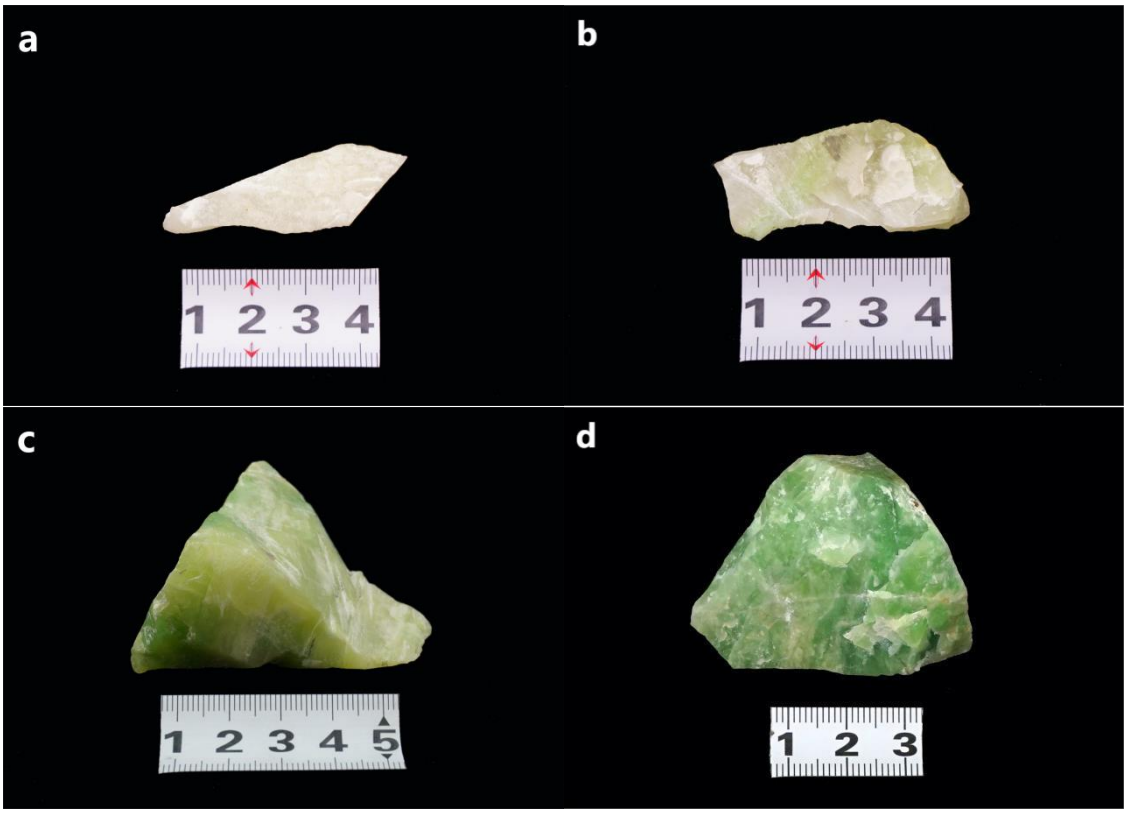

Figure 1. Sample photographs. **(a)** ZB-3: White patches within a white matrix. **(b)** ZB-2: Fibrous green inclusions embedded in a white matrix. **(c)** ZB-1: Yellowish-green matrix containing white veinlets, emerald-green spots, and fibrous green inclusions. **(d)** ZB-4: Light green matrix exhibiting dark green patches, fibrous green inclusions, and white veinlets.

The major element composition of both the matrix and specific surface features of the samples was analyzed using an EPMA-1600 electron probe microanalyzer (Shimadzu Corporation) at the Electron Microprobe Laboratory of the China University of Geosciences, Beijing(CUGB). Measurements were carried out under an accelerating voltage of 15 kV, a beam current of 1×10^{-8} A, and a beam diameter of 1 μm. Natural mineral standards were used for calibration, and the detection limits for major elements were below 0.01 wt%.

Ultraviolet-visible (UV-Vis) spectroscopy was performed using a GEM-3000 fiber optic spectrometer (Guangzhou Biaoqi Electronics Technology Co., Ltd.) at the National Infrastructure of Mineral, Rock, and Fossil Resources for Science and Technology (NIMRF). The measurements were carried out with an integration time of 60 ms, 20 averaged scans, a smoothing width of 5 nm, and a spectral range of 400–700 nm.

Elemental distribution mapping of the polished thin sections was performed using an X-ray fluorescence (XRF) spectrometer at the National Infrastructure of Mineral, Rock, and Fossil Resources for Science and Technology (NIMRF). The system was operated at 50 KV and 300 μA, with a spot size of 30 μm and a stage speed of 20 ms/s.

Fourier-transform infrared (FTIR) spectroscopic analysis was conducted at the National Infrastructure of Mineral, Rock, and Fossil Resources for Science and Technology (NIMRF), using a BRUKER TENSOR II spectrometer. Measurements were carried out at a temperature of 24 °C and a relative humidity of 22%, over a wavenumber range of 400–4000 cm^{-1} with a resolution of 4 cm^{-1} and 32 accumulated scans.

 doi:10.20944/preprints202509.1587.v1

3. Results

3.1. Conventional Gemological Properties

Zibai Jade exhibits a massive texture and ranges from translucent to semi-translucent. It has a refractive index of 1.71–1.72 (spot method) and a specific gravity of 3.40–3.54. The samples display heterogeneous color distribution. In addition to a base coloration of light green and yellowish-green, the surface exhibits characteristic features such as emerald-green spots, dark green spots, fibrous green inclusions, white patches, white veinlets, and black dot with a green ring (Figure 2). The overall coloration of the samples is predominantly influenced by these surface features. The conventional gemological parameters of the four samples are summarized in Table 1.

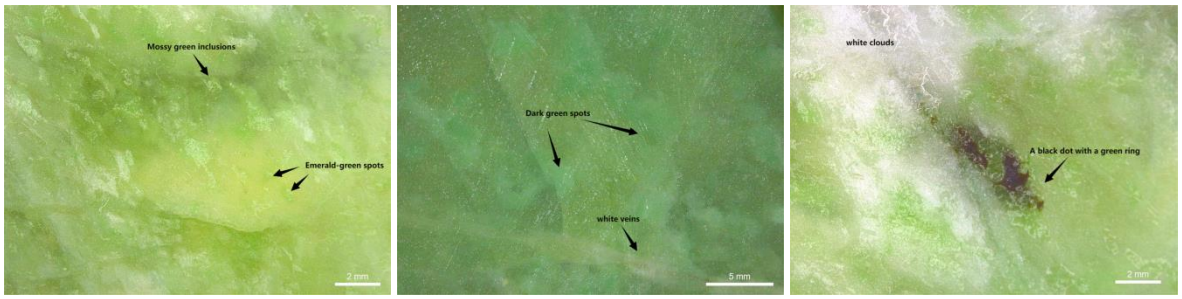

(a) **(b)** **(c)**

Figure 2. Surface Characteristics of the Samples. (**a**)Mossy green inclusions and Emerald-green spotsd. (**b**)Dark green spots and white veins (**c**)White clouds and a black dot with a green ring.

Table 1. Gemological Parameters of Zibai Jade Samples.

Sample Number	Color	Refractive Index	Specific Gravity	UV Fluorescence (LW/SW)	Chelsea Filter Response
ZB-1	Yellowish-green	1.71	3.44	None	Turns red
ZB-2	White	1.72	3.53	None	Light red
ZB-3	Light green	1.72	3.54	None	Light red
ZB-4	Dark green	1.71	3.40	None	Turns red

3.2. X-Ray Powder Diffraction (XRD)

Analyses were performed on the pure white matrix of the white hydrogrossular jade sample ZB-3. The diffraction data of the sample were processed using MDI Jade 6.5 software, and the resulting diffraction pattern was compared with standard reference patterns from the JCPDS database using PDF cards for phase identification (Figure 3). The major diffraction peaks of the hydrogrossular jade sample ZB-3 match well with the reference pattern of grossular (PDF#79-1267, Grossular ferroan), while partial peak correspondence is also observed with vesuvianite (PDF#87-1119, Vesuvianite). These results indicate that the pure white matrix of ZB-3 is primarily composed of grossular, with minor amounts of vesuvianite, which is consistent with observations under polarizing microscopy. The sharp diffraction peaks indicate a highly crystalline and fine-grained nature of the sample. The corresponding diffraction data are provided in Table 2.

Table 2. Comparison of X-ray Powder Diffraction Data for Hydrogrossular Jade Sample ZB-3 with Standard PDF Cards.

	ZB-3			Phase Identification	PDF#79-1267 Grossular ferroan			PDF#87-1119 Vesuvianite		
(hkl)	2θ	d(Å)	I%		2θ	d(Å)	I%	2θ	d(Å)	I%
(400)	30.122	2.9644	33.8	Grossular	30.143	2.9623	37.7			

 doi:10.20944/preprints202509.1587.v1

(432)	32.595	2.7449	6.5	Vesuvianite				32.523	2.7508	100
(420)	33.78	2.6512	100	Grossular	33.802	2.6496	100			
(224)	34.46	2.6004	2.7	Vesuvianite				34.419	2.6035	37.3
(522)	34.634	2.5878	3.1	Vesuvianite				34.561	2.5931	56.1
(332)	35.481	2.5279	7.3	Grossular	35.505	2.5263	6.3			
(620)	36.643	2.4504	2.5	Vesuvianite				36.543	2.4569	40.8
(422)	37.118	2.4201	16.7	Grossular	37.14	2.4187	20.2			
(431)	38.697	2.3250	16.6	Grossular	38.716	2.3238	13.2			
(521)	41.697	2.1643	14.2	Grossular	41.716	2.1634	12.1			
(440)	43.135	2.0955	3.6	Grossular	43.152	2.0947	2.6			
(611)	47.222	1.9232	24	Grossular	47.247	1.9222	19.1			
(620)	48.535	1.8742	1.6	Grossular	48.552	1.8735	1.4			
(444)	53.516	1.7109	17.2	Grossular	53.536	1.7103	12.9			
(640)	55.881	1.6439	23.2	Grossular	55.909	1.6432	22.5			
(642)	58.197	1.5839	39.6	Grossular	58.217	1.5834	36.1			
(800)	62.641	1.4818	8.7	Grossular	62.671	1.4812	8.2			

The powder diffraction data of hydrogrossular jade sample ZB-3 were subjected to angle calibration and least-squares refinement using MDI Jade 6 software to calculate its unit cell parameters. These parameters were then compared with those of standard mineral reference patterns from the PDF database (Table 3). The results indicate that the unit cell parameters of the sample show relatively significant deviations from those of the reference pattern PDF#79-1267 (Grossular ferroan). This discrepancy may be attributed to the presence of a small amount of structural water in the sample, further confirming that the pure white matrix of the hydrogrossular jade is primarily composed of hydrogrossular.

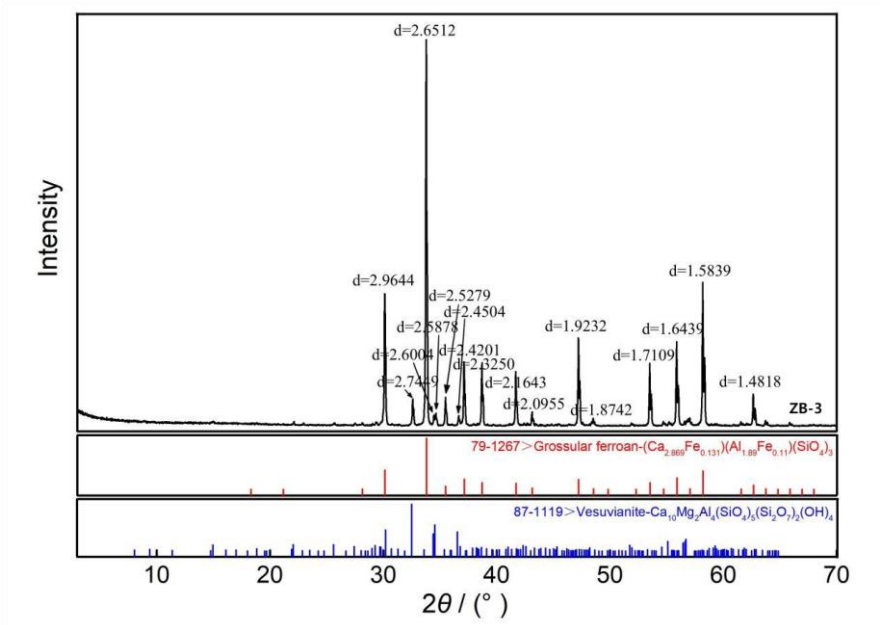

Figure 3. X-ray Diffraction Pattern of Hydrogrossular Jade (Sample ZB-3).

Table 3. Comparison of Unit Cell Parameters Between Hydrogrossular Jade Sample ZB-3 and Reference PDF Cards.

Sample	Axis a (Å)	Axis b (Å)	Axis c (Å)	Angle α (°)	Angle β (°)	Angle γ (°)
ZB-3	11.493	11.493	11.493	90.000	90.000	90.000

 doi:10.20944/preprints202509.1587.v1

PDF#79-1267 Grossular ferroan	11.849	11.849	11.849	90.000	90.000	90.000

3.3. Microstructural Characteristics

Under polarizing microscopy, the white and light green matrix of the jade was observed to consist of fine-grained hydrogrossular and vesuvianite, with hydrogrossular accounting for approximately 82% of the composition.Hydrogrossular occurs as fine-grained particles with indistinct boundaries, exhibiting complete extinction under cross-polarized light and weak interference colors in some grains. Vesuvianite forms granular crystals of small size, with a few individuals displaying relatively well-formed crystal shapes. Under plane-polarized light, the mineral is colorless and exhibits moderate to high relief with distinct surface roughness. Under cross-polarized light, it displays anisotropic characteristics with first-order gray interference colors. Anomalous interference colors are observed, including yellowish-brown, indigo blue, grayish-green, lilac, and turbid white (Figure 4a). The emerald-green spots are identified as uvarovite. Under cross-polarized light, they exhibit complete extinction, while under plane-polarized light, they display a vivid green color. These minerals occur as granular crystals embedded within the matrix of the jade (Figure 4b). The dark green sports are identified as diopside grains partially replaced by hydrogrossular and chlorite. Under plane-polarized light, they appear colorless with moderate to high relief; under cross-polarized light, they exhibit anisotropic characteristics with second-order blue-green to orange-yellow interference colors. Replacement by hydrogrossular occurs along cleavage planes, with partial alteration to chlorite (Figure 4c). The mossy green inclusions are predominantly composed of chlorite and Cr-bearing grossular. Chlorite occurs as fine-scaly aggregates, appearing colorless to pale green under plane-polarized light with low relief. Under cross-polarized light, it exhibits anisotropic properties with first-order gray to gray-white interference colors. Cr-bearing grossular appears colorless to pale green under plane-polarized light and exhibits complete extinction under cross-polarized light (Figure 4d). The white veinlets and patches are identified as calcite. Under plane-polarized light, it appears colorless and exhibits distinct twinkling relief. Under cross-polarized light, it shows anisotropic properties with high-order white interference colors（Figure 4e、Figure 4f）.

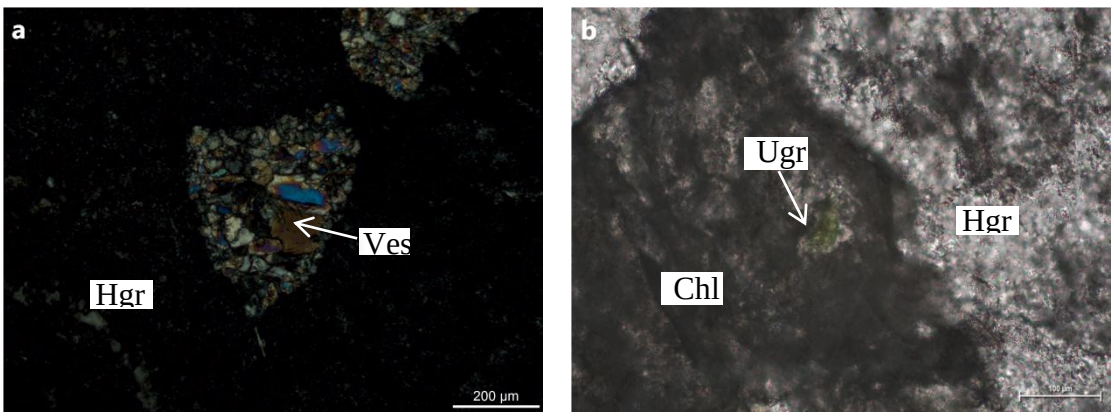

 doi:10.20944/preprints202509.1587.v1

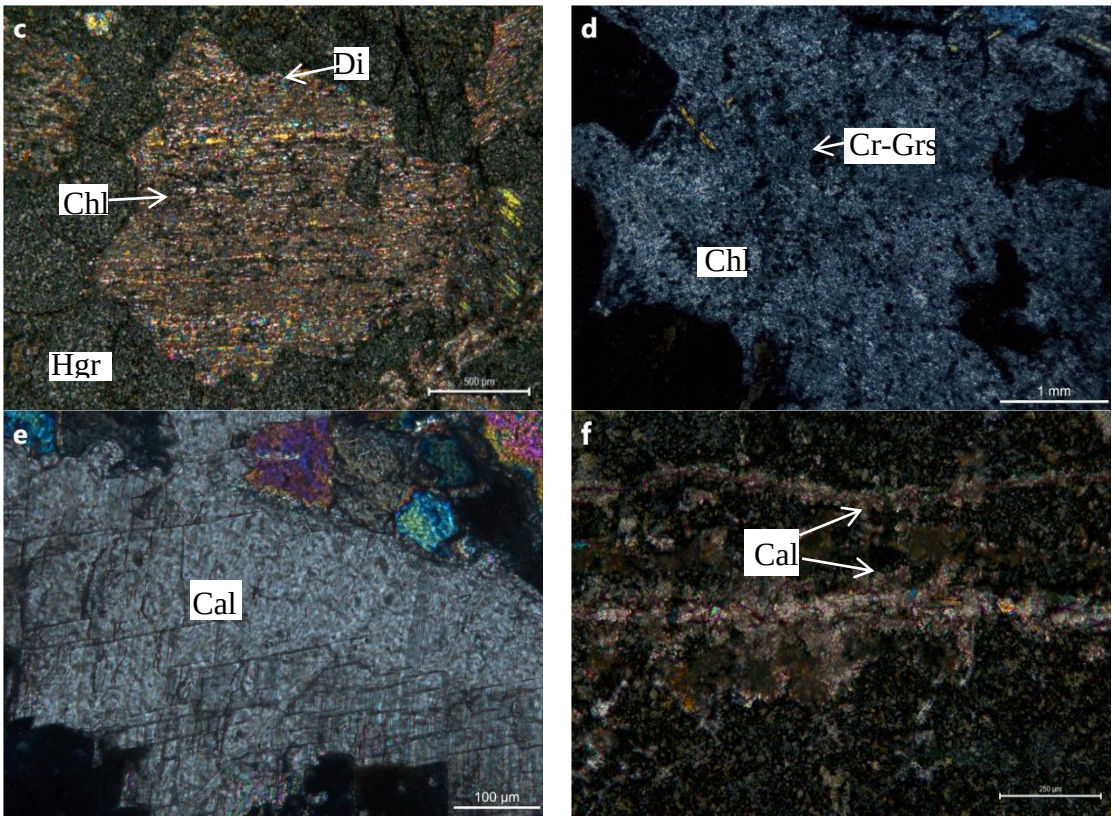

Figure 4. Polarizing Micrographs of the Samples. (**a**)Hydrogrossular occurs in the matrix alongside relatively larger vesuvianite grains (+). (**b**)Uvarovite exhibiting an emerald-green coloration (-) (**c**)Diopside grains are replaced by hydrogrossular along cleavage planes, with partial alteration to chlorite (+). (**d**)Chlorite and Cr-bearing grossular. (**e**)Coarse-grained calcitez(+). (**f**)Calcite veinlets (+).

3.4. Backscattered Electron (BSE) Images

Backscattered Electron (BSE) imaging provides a clear and intuitive representation of the interrelationships between minerals, particularly through compositional contrast and well-defined phase boundaries. The emerald-green spots are composed of uvarovite, with edges altered by hydrogrossular, suggesting that they originated from the alteration of earlier-formed chromite. (Figure 5a). The dark green Sports are primarily composed of diopside as a host mineral. During low-temperature alteration, portions of the diopside were transformed into chlorite, releasing elements such as Ca and Si. These elements subsequently reacted with Al-rich fluids, leading to the precipitation of hydrogrossular along the cleavage planes of the diopside (Figure 5b). The mossy green inclusions are primarily composed of chlorite and chromium-bearing grossular, which are distributed within the hydrogrossular-dominated matrix (Figure 5c). Two generations of calcite are recognized: early relict patches derived from the protolith during metasomatism, appearing as white spots, and late-stage veinlets cutting through the matrix, manifested as white veinlets (Figure 6d, Figure 5e). The black cores with green rims texture is interpreted as the replacement of chromite by uvarovite, suggesting an alteration process from primary chromite to secondary chromium-rich garnet (Figure 5f).

 doi:10.20944/preprints202509.1587.v1

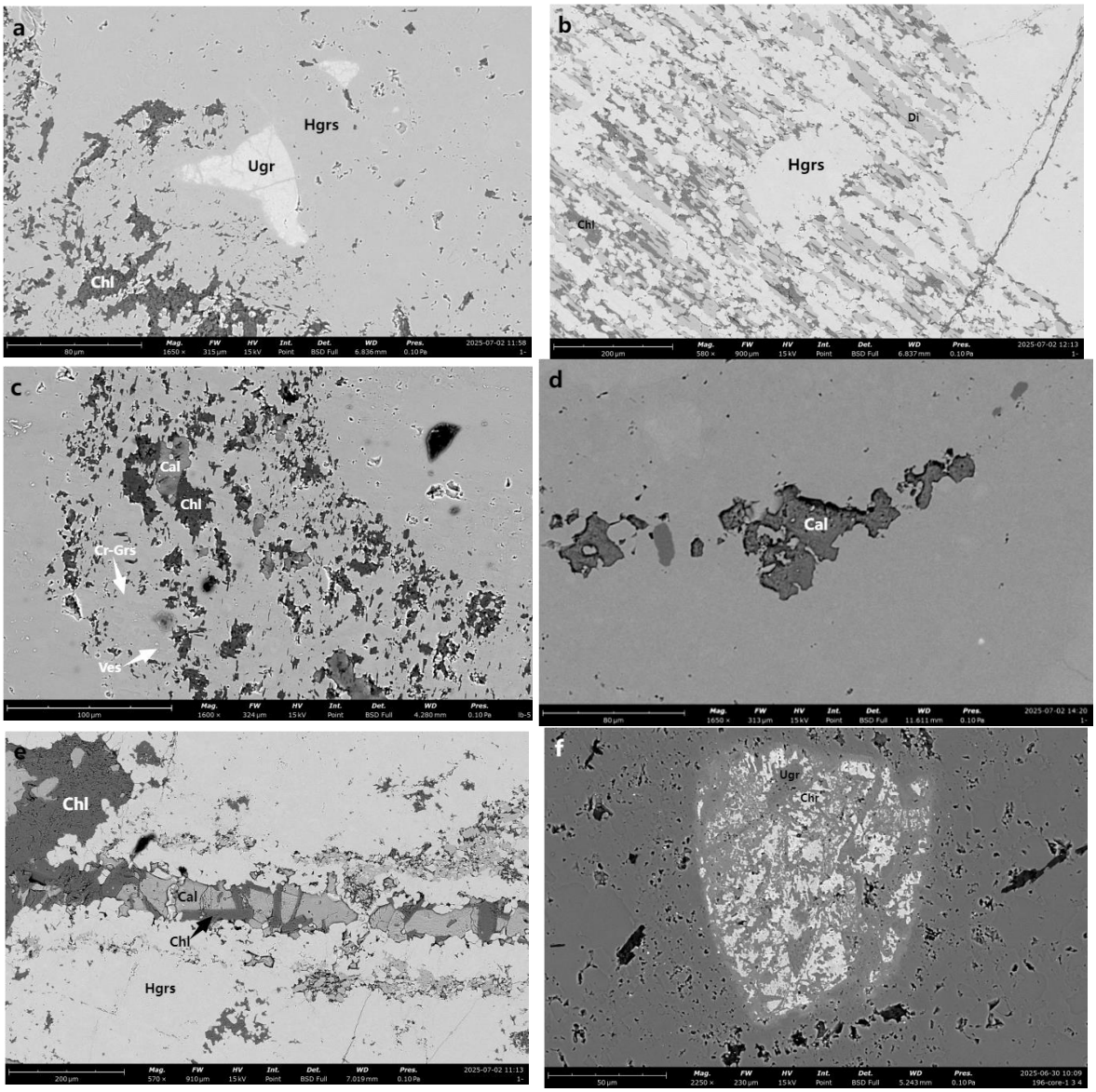

Figure 5. Backscattered Electron (BSE) Images. (**a**)emerald-green spots. (**b**)dark green spots (**c**)Mossy green inclusions (+). (**d**)white patches. (**e**)white veinlets. (**f**)black dot with a green ring.

3.5. EPMA

Previous tests revealed that the green areas of the sample turned red under the Chelsea colour filter (CCF). This phenomenon is attributed to the presence of Cr^{3+}, which undergoes six-coordinated isomorphic substitution for Al^{3+} in octahedral sites, resulting in the green coloration of the material [14]. Based on the electron probe microanalysis (EPMA) results, which indicate relatively high concentrations of chromium and iron in the sample, it is preliminarily suggested that the green coloration is primarily attributed to Cr^{3+} and Fe [15].

The hydrogrossular and vesuvianite in the matrix contain almost no chromium but differ primarily in iron content: hydrogrossular contains exclusively Fe^{3+}, whereas vesuvianite hosts only Fe^{2+}. The combined effect of these two iron valence states imparts a yellowish-green hue to the matrix of the jade. The emerald-green spots in the jade exhibit a chromium content as high as 10.43 wt%, which is identified as the primary chromogenic element responsible for their distinctive coloration. Fe^{3+} is also predominantly concentrated in chlorite, which is the primary chromogenic element responsible for the dark green coloration in the jade.A sharp chromium gradient zone was observed in the “black dot with a green ring” texture, with Cr content decreasing from 18.17 wt% to 11.88 wt% as the distance from the chromite core increases. Detailed data are provided in Table 4.

 doi:10.20944/preprints202509.1587.v1

Table 4. Chemical Composition of Constituent Minerals in the Jade.

Sample / Date	Matrix		emerald-green spots	dark green spots		
	ZBJ-1(Hgrs)	ZBJ-2(Ves)	ZBC-1(Ugr)	ZBS-1(Di)	ZBS-2(Chl)	ZBS-3(Hgrs)
SiO2	37.54	35.26	35.18	53.54	23.06	35.27
Na2O	0.00	0.04	0.07	0.05	0.04	0.05
TiO2	0.05	0.04	0.15	0.00	0.04	0.00
MgO	0.14	3.26	0.05	19.10	30.90	0.06
K2O	0.00	0.02	0.01	0.00	0.01	0.01
Al2O3	24.13	17.76	12.69	0.34	30.51	21.71
CaO	36.41	38.13	35.98	25.34	0.03	38.75
Cr2O3	0.02	0.03	10.43	0.08	0	0.00
MnO	0.01	0.09	0.09	0.04	0.06	0.00
Fe2O3	0.38	—	3.27	0.59	3.31	0.44
FeO	—	1.62	—	—	—	—
NiO	0.05	0.00	0.00	0.00	0.32	0.00
CoO	0.00	0.00	0.02	0.00	0.04	0.00
Total	98.73	96.25	97.94	99.08	88.32	96.29
Sample / Date	**Mossy green inclusions**		**black dot with a green ring**			
	ZBX-1(Chl)	ZBX-2(Cr-Grs)	ZBH-1(Chr)	ZBH-2(Ugr)	ZBH-3(Ugr)	ZBH-4(Ugr)
SiO2	26.01	35.80	0.44	34.17	33.92	34.18
Na2O	0.08	0.07	0.19	0.05	0.04	0.06
TiO2	0.01	0.60	0.00	0.20	0.31	0.56
MgO	31.44	0.44	2.41	0.04	0.06	0.13
K2O	0.07	0.04	0.03	0.01	0.00	0.03
Al2O3	22.72	18.38	10.55	6.71	8.55	10.63
CaO	3.77	35.14	1.31	35.13	35.12	35.03
Cr2O3	0.08	1.41	44.36	18.17	15.99	11.88
MnO	0.07	0.38	1.35	0.16	0.17	0.17
Fe2O3	1.95	3.01	13.09	1.86	2.85	3.65
FeO	—	—	26.21	—	—	—
NiO	0.19	0.00	0.36	0.01	0.00	0.00
CoO	0.08	0.02	0.24	0.01	0.02	0.00
Total	86.47	95.25	100.54	96.52	97.03	96.32

3.6. UV-Vis

For this study, four distinct regions of the jade exhibiting gradational coloration from light to dark were selected and subjected to ultraviolet-visible (UV-Vis) spectroscopic analysis (Figure 6). Two strong and broad absorption bands are observed in the ranges of 400–460 nm and 570–670 nm, accompanied by a weak absorption peak at 457 nm. These features indicate selective absorption of violet-blue and yellow-orange light, resulting in the green coloration of the sample. The absorption band observed between 400–460 nm is attributed to electronic transitions between split energy levels resulting from the division of the 5D spectroscopic term in the $3d^6$electron configuration of Fe^{2+}. In an octahedral field, the only allowed electronic transition for Fe^{2+} is $^5T_2g \rightarrow {}^5Eg$ [16]. The absorption band at 570-670 nm is primarily attributed to the typical spin-forbidden d-d transition of Cr^{3+} in octahedral coordination, specifically $^4A_2g(F) \rightarrow {}^4T_2g(F)$, superimposed on the absorption resulting from charge transfer between $Fe2^+$ and Fe^{3+} [17]. The shoulder peak at 457 nm is attributed to energy level splitting caused by octahedral distortion of Cr^{3+} [18,19]. Therefore, the primary chromogenic elements in Zibai Jade are Cr^{3+} and Fe.

 doi:10.20944/preprints202509.1587.v1

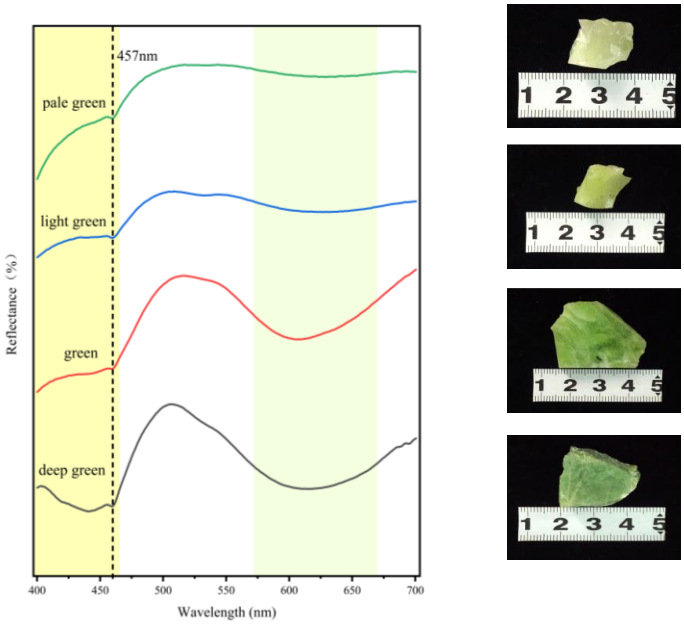

Figure 6. UV-Vis Spectra and Four Regions with Varying Coloration.

3.7. XRF

To visually observe the distribution of chromogenic elements Cr and Fe in Zibai Jade, polished sections containing emerald-green spots, dark green patches, and fibrous green inclusions were subjected to μ-XRF mapping analysis. The scanning results are presented in the figure below (Figure 7). Combined Cr and Fe elemental distribution maps reveal that the matrix of the jade is nearly devoid of Cr, while Fe is predominantly concentrated in chlorite-rich regions. These observations are consistent with the results obtained from SEM and EPMA. Areas with the highest Cr concentration, indicated by red zones on the map, exhibit distinct point-like distributions that correspond to the emerald-green spots within the jade. Minor Cr enrichment is also observed in chlorite and Cr-bearing grossular, aligning with the distribution of fibrous green inclusions.

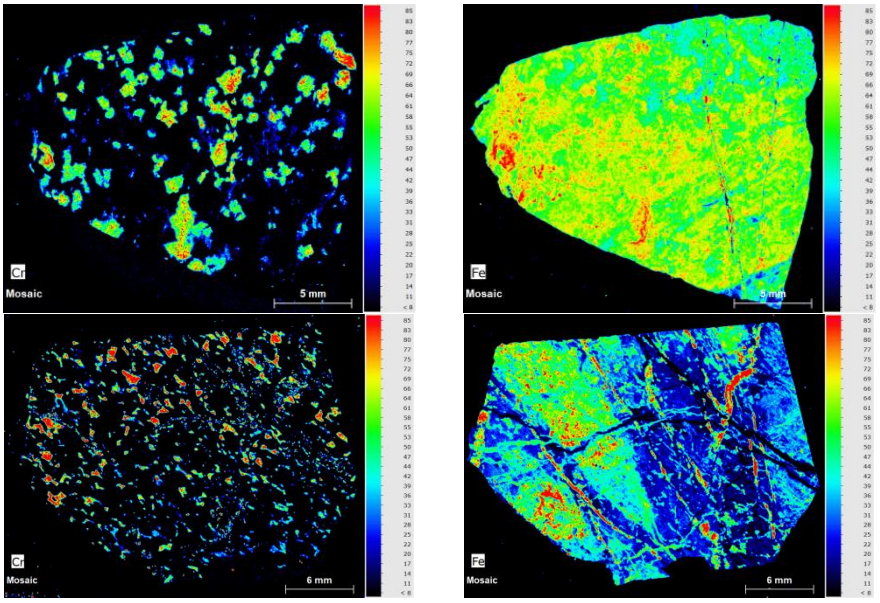

Figure 7. Cr and Fe Elemental Distribution Maps.

 doi:10.20944/preprints202509.1587.v1

3.8. FTIR

The characteristic infrared absorption bands of Zibai Jade are primarily observed in the regions of 3700-3600 cm^{-1}, 1000-800 cm^{-1}, and 700-400 cm^{-1}(Figure 8). Compared with the reference infrared spectrum of grossular from the RRUFF database, the sample exhibits a νO—H stretching vibration in the range of 3700-3600 cm^{-1} and a δO—H bending vibration at 1641 cm^{-1}. These observations are attributed to the presence of structural OH groups in the sample [20][21]. Hydrogrossular has the chemical formula $Ca_3Al_2[SiO_4]_{3-x}(OH)_{4x}$ and belongs to the nesosilicate mineral group. According to previous studies, absorption bands above 500 cm^{-1} may be related to asymmetric stretching and bending vibrations of SiO_4 groups, while bands below 500 cm^{-1} are primarily influenced by trivalent and divalent cations [22]. The absorption peaks at 1097, 862, and 844 cm^{-1} are assigned to the ν_{as} Si-O-Si asymmetric stretching vibration. The peak at 619 cm^{-1} corresponds to the ν_3Cr-O stretching vibration, while the peak at 544 cm^{-1} is attributed to the ν_2O-Cr-O bending vibration. The peak at 476 cm^{-1} is assigned to the ν_1Fe-O stretching vibration, and the peak at 458 cm^{-1} is associated with lattice vibrations (related to Al^{3+} vibrations) [23][24]. The absorption peak at 3670 cm^{-1} is attributed to the νO-H stretching vibration [25], and the peak at 1647 cm^{-1} corresponds to the δO-H bending vibration. The absorption peak at 1422 cm^{-1} may be caused by chlorite present in the jade [26].

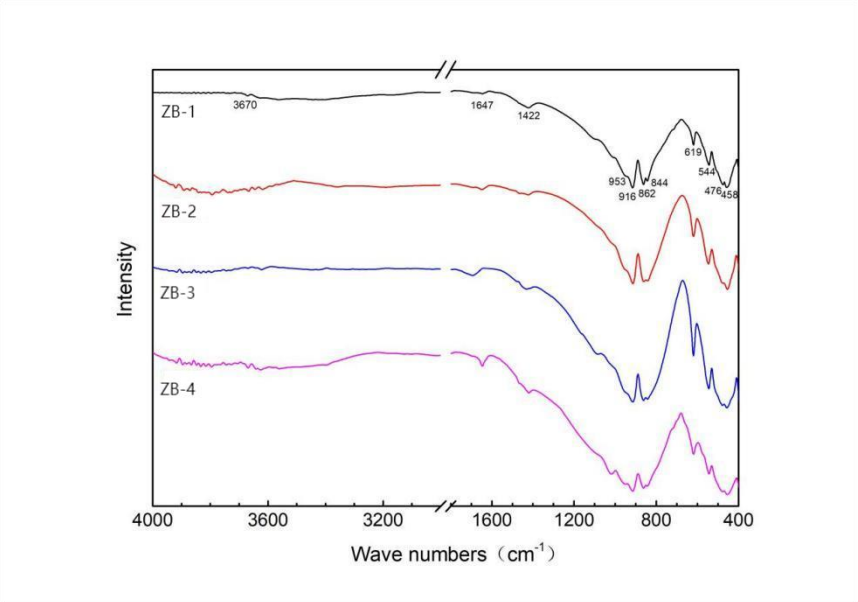

Figure 8. Infrared Spectrum of Zibai Jade.

Table 5. Infrared Spectral Characteristics and Assignments of Hydrogrossular Jade (ZB-1).

Sample / Vibrational Mode Assignments	ZB-1
ν_{as} Si-O-Si Asymmetric Stretching Vibration	1097cm^{-1}，862cm^{-1}，844cm^{-1}
ν_3 Cr-OStretching Vibration	619cm^{-1}
ν_2O-Cr-OBending Vibration	544cm^{-1}
ν_1Fe-OStretching Vibration	476cm^{-1}
Lattice Vibrations (Associated with Al^{3+} Vibrations)	458cm^{-1}
NO-H Stretching Vibration	3670cm^{-1}
δ O-H Bending Vibration	1647cm^{-1}

 doi:10.20944/preprints202509.1587.v1

4. Discussion

4.1. Mineralogical Characteristics and Formation Mechanism

Based on comprehensive analyses including conventional gemological testing, X-ray diffraction (XRD), polarizing microscopy, and backscattered electron (BSE) imaging, Zibai Jade is identified as a jade predominantly composed of hydrogrossular, with minor amounts of vesuvianite, uvarovite, diopside, chlorite, calcite, and chromite. Based on the geological context and analytical results, it can be concluded that Zibai Jade is a typical product of multi-stage hydrothermal metasomatism and retrograde alteration of calc-silicate skarn. Its formation can be divided into three distinct stages, controlled synergistically by protolith composition, hydrothermal activity, and temperature-pressure conditions.

Stage 1: Protolith Accumulation

Zibai Jade is located on the northwestern margin of the South Qinling Orogenic Belt. Its protolith is proposed to have been derived from calcium-rich carbonate rocks (dolomite or limestone), which provided the essential material foundation for the formation of the jade.

Stage 2: High-Temperature Metasomatic Stage

This stage represents the main period of jade formation. Silica- and alumina-rich hydrothermal fluids metasomatized the carbonate rocks, leading to the crystallization of grossular and diopside. The diopside occurs as short-prismatic crystals embedded within the grossular-dominated matrix. Simultaneously, chromium-rich hydrothermal fluids derived from mafic–ultramafic rocks formed large chromite grains coexisting with grossular. As the temperature of the hydrothermal fluids decreased, grossular reacted with Mg, Si, and other components to form vesuvianite grains. Chromite was progressively replaced by uvarovite, resulting in the characteristic “black-core-with-green-rim” texture. The white patches in the jade are composed of isolated calcite, representing relict fragments of the carbonate protolith.

Formation of Grossular：

$3CaCO_3+Al_2O_3+3SiO_2 \rightarrow Ca_3Al_2(SiO4)_3+3CO_2 \uparrow$

Crystallization of Diopside：

$2CaCO_3+MgCO_3+4SiO_2 \rightarrow 2CaMgSi2O_6+3CO_2 \uparrow$

Formation of Uvarovite：

$(Fe, Mg)Cr_2O_4+3CaO+3SiO_2 \rightarrow Ca_3Cr_2(SiO_4)_3+(Fe, Mg)O$

Formation of Vesuvianite:

$5Ca_2Al_2(SiO_4)_3(OH)_4+2SiO_2+2MgO+2H_2O \rightarrow 2Ca_{10}Mg_2Al_4(SiO_4)_5(Si_2O_7)_2(OH)_4$

Stage 3: Retrograde Alteration Stage

During this stage, the jade was percolated by late-stage CO_2/H_2O-rich fluids along fractures, leading to the alteration and reorganization of early-stage minerals. Grossular was hydrated to form hydrogrossular, while completely altered chromite was transformed into uvarovite, producing emerald-green spots. Diopside was altered to chlorite, constituting the dark green patches on the jade surface. The released Ca and Si reacted with Al-rich fluids, precipitating hydrogrossular along fractures in diopside [27]. As temperatures gradually decreased, aqueous fluid activity intensified, promoting the conversion of grossular to hydrogrossular. A minor portion of Cr^{3+} released from diopside substitutionally replaced Al^{3+} in the hydrogrossular lattice. CO_2-rich fluids dissolved and reprecipitated carbonates, forming secondary calcite veinlets manifested as white veins on the jade surface.

Diopside is altered to chlorite.：

$5CaMgSi_2O_6+4H_2O+2CO_2 \rightarrow Mg_5Al\ (AlSi_3O_{10})\ (OH)_8+5CaCO_3+7SiO_2$

Grossular is hydrated to hydrogrossular [28]：

$Ca_3Al_2(SiO_4)_3+2XH_2O \rightarrow Ca_3Al_2\ (Si\ O_4)_{\ 3-x}(OH)_{4x}+XSiO_2$

 doi:10.20944/preprints202509.1587.v1

4.2. Chromogenic Mechanism

Combined data from ultraviolet-visible (UV-Vis) spectroscopy, infrared (IR) spectroscopy, and electron probe microanalysis (EPMA) indicate that the coloration of Zibai Jade is primarily attributed to absorption transitions related to Fe^{3+}, Fe^{2+}, and Cr^{3+}. IR spectroscopy further detected vibration peaks associated with both iron and chromium elements. UV-Vis spectroscopy directly reflects the absorption characteristics of iron and chromium elements. The yellowish-green hue of the jade is primarily caused by electronic transitions of iron and chromium at 300–380 nm, 400–460 nm, and 570–670 nm, leading to selective light absorption in these ranges. The green coloration of the sample results from the selective absorption of violet-blue and yellow-orange light. Combined EPMA and XRF mapping clearly delineate the distribution of iron and chromium elements. The matrix of the jade is nearly devoid of chromium and primarily exhibits a yellowish-green hue derived from iron in hydrogrossular and vesuvianite. Chromium is predominantly concentrated in uvarovite, forming the emerald-green spots on the jade surface. Iron is mainly hosted in chlorite, contributing to dark green sports and fibrous green inclusions. The characteristic "black-core-with-green-rim" texture results from the replacement of chromite by uvarovite. White patches and veinlets in the jade are attributed to relict carbonate minerals from the high-temperature mineralization stage and late-stage calcite veins formed during low-temperature alteration.

5. Conclusions

Through conventional gemological testing and multiple modern analytical techniques, the mineralogical characteristics, coloration mechanism, and formation process of Zibai Jade have been determined, leading to the following conclusions:

(1) Zibai Jade exhibits heterogeneous color distribution, featuring a base of light green and yellowish-green tones along with characteristic surface occurrences such as dark green patches, fibrous green inclusions, white patches, white veinlets, and black-core-with-green-rim textures. The sample has a refractive index of 1.71-1.72, a specific gravity of 3.40-3.54, shows no reaction to ultraviolet fluorescence, and turns red under the Chelsea filter.

(2) The jade is primarily composed of hydrogrossular, which constitutes over 82% of the matrix. Minor minerals include diopside, vesuvianite, chlorite, uvarovite, calcite, and chromite.

(3) The coloration of the jade is primarily governed by the combined effects of iron and chromium elements. The emerald-green spots consist of uvarovite, while the dark green sports are composed of diopside, hydrogrossular, and chlorite, with diopside being partially altered to chlorite. The fibrous green inclusions are predominantly formed by chlorite and Cr-bearing grossular. The white patches and veinlets are composed of carbonate minerals, predominantly calcite. The "black dot with a green ring" texture is mainly constituted by chromite and uvarovite.

(4) The formation of the jade involved three mineralization stages: protolith accumulation, high-temperature metasomatism, and retrograde alteration. The synergistic interaction of these processes resulted in the development of Zibai Jade, which exhibits a dense texture and attractive coloration.

Author Contributions: Conceptualization, M.H.; methodology, M.H. and L.S.; software, L.S. and Z.Z.; formal analysis, L.S., Z.Z. and L.Y.; investigation, L.S. and Z.Z.; data curation, L.S.; writing—original draft preparation, L.S and Z.Z.; writing—review and editing, M.H.; supervision, M.H.; All authors have read and agreed to the published version of the manuscript.

Funding: National Mineral Rock and Fossil Specimens Resource Center

Institutional Review Board Statement: Not applicable.

Informed Consent Statement: Not applicable.

Data Availability Statement: The original contributions presented in this study are included in the article. Further inquiries can be directed to the corresponding author.

Acknowledgments: We thank Shaanxi Dikan Hanyuan Jade Industry Co., Ltd. (Shaanxi,China) for providing samples for this study. We thank the laboratory of the National Mineral Rock and Fossil Specimens.

Conflicts of Interest: The authors declare no conflicts of interest.

References

1. Zhao, D.T. Analysis of Natural Jade Resources in Qinghai Province. J. Qinghai Univ. (Nat. Sci. Ed.) **2012**, *30*, 66–68+75. doi: 10.13901/j.cnki.qhwxxbzk.2012.04.014.
2. Li, Z.C. Garnet. Zhu Bao **1991**, *2*, 16–19+1.
3. Zheng, Y.L.; Chen, M.H.; Sun, R.Z.; et al. Gemological and Mineralogical Characteristics of Pink Hydrogrossular. J. Gems Gemmol. **2023**, *25* (1), 14–20. doi: 10.15964/j.cnki.027jgg.2023.01.002.
4. Hsu, T.; Kennedy, L.; Choudhary, G. Synthetics and Simulants. Gems Gemol. **2024**, *60*, 260–265.
5. Chilstrom, C. Large Star Emerald. Gems Gemol. **2015**,*51* (3), pp. 334–335.
6. Xu, Y.R. Study on Gemological and Mineralogical Characteristics of Hydrogrossular Jade and Vesuvianite Jade from the Tawmaw Area, Myanmar. Master's Thesis, China University of Geosciences (Beijing), Beijing, China, 2014.
7. Lu, R. Three Similar-Appearing Green Stones: Jadeite, Omphacite, and Hydrogrossular. Gems Gemol. **2011**,*47* (1), pp. 52–53.
8. Liu, H.; Ruan, Q.F.; Qiu, Z.H.; et al. Mineralogical Characteristics and Color Genesis of Vesuvianite Jade from Hanzhong, Shaanxi Province. Mineral. Petrol. **2023**, *43* (3), 1–9. doi: 10.19719/j.cnki.1001-6872.2023.03.01.
9. Zhang, Y.J.; Liang, W.T.; Luo, X.R.; et al. Geochemical Characteristics and Petrogenetic Significance of Biotite from Guangtoushan Rock Masses, Qinling Orogenic Belt. Mineral. Petrol. **2015**, *35* (1), 100–108. doi: 10.19719/j.cnki.1001-6872.2015.01.013.
10. Song, X.W.; Hou, M.T.; Chen, R.Y. Division of Metallogenic Provinces (Belts) in Shaanxi Province. Northwest. Geol. **2004**, *3*, 29–42.
11. Wang, F.; Li, J.Y.; Fu, C.; et al. Geological Characteristics and Gold Prospecting Potential of the Pogenjiao Silver-Lead Deposit in Taibai County, Shaanxi Province. Acta Geol. Sichuan **2017**, *37* (3), 396–399+420.
12. Wang, Z.M.; Xiao, H.L.; Wang, D.S.; et al. Geological Characteristics and Metallogenic Conditions of the Xigou Copper Deposit in Liuba County, Shaanxi Province. Shaanxi Geol. **2018**, *36* (2), 15–18.
13. Fang, Z.; Wang, X.M. Mineralogical Study of the Jade "Budaweng" Resembling Jadeite. Geol. Chem. Miner. **2002**, *1*, 7–10+27.
14. Liang, T.; Liu, Y.X. Comparative Study of Color Characteristics of Yunnan Emerald and Colombian Emerald. J. Xi'an Eng. Univ. **1998**, *3*, 43–47.
15. Tian, H.S.; Zhao, Y.J. Discovery and Preliminary Study of Chromium-rich Vesuvianite from Yaoshan, Jinan. Shandong Geol. **1992**, *2*, 115–118.
16. Wu, H.Q. Study on Gemological Characteristics and Color Genesis of Orange-Red Series Garnet. Master's Thesis, China University of Geosciences, Beijing, China, **2016**.
17. Li, M.Y. Gemological Characteristics and Color Genesis of Philippine "Dushan Jade". Master's Thesis, China University of Geosciences, Beijing, China, **2019**. doi: 10.27493/d.cnki.gzdzy.2019.000617.
18. Liu, J.; Yang, M.X.; Di, J.R.; et al. Spectroscopic Study of Uvarovite in Anorthite Jade. Spectrosc. Spect. Anal. **2018**, *38* (6), 1758–1762. doi: 10.3964/j.issn.1000-0593(2018)06-1758-05.
19. Qu, M.W.; Zhong, Y.; Shen, X.T. Gemological Characteristics of Zambian Purplish-Red to Brownish-Red Garnets. J. Gems Gemmol. **2021**, *23* (4), 20–28. doi: 10.15964/j.cnki.027jgg.2021.04.003.
20. Schoenitz, M.; Navrotsky, A. Enthalpy of Formation of Katoite $Ca_3Al_2[(OH)_4]_3$: Energetics of the Hydrogarnet Substitution. Am. Mineral. **1999**, *84* (3), 389–395.
21. Geiger, C.A.; Dachs, E.; Benisek, A. Thermodynamic Behavior and Properties of Katoite (Hydrogrossular): A Calorimetric Study. Am. Mineral. **2012**, *97* (7), 1252–1255.
22. Panikorovskii, T.L.; Krivovichev, S.V.; Galuskin, E.V.; et al. Si-Deficient, OH-Substituted, Boron-Bearing Vesuvianite from Sakha-Yakutia, Russia: A Combined Single-Crystal, 1H MAS-NMR and IR Spectroscopic Study. Eur. J. Mineral. **2016**, *28* (5), 931–941.

23. Liu, X. Study on Gemological and Mineralogical Characteristics of Henan Dushan Jade. Master's Thesis, Hebei GEO University, Shijiazhuang, China, 2022. doi: 10.27752/d.cnki.gsjzj.2022.000839.
24. Yong, C.Y. Study on Gemological and Mineralogical Characteristics of Mexican Strawberry-Red Grossular Garnet. Master's Thesis, China University of Geosciences, Beijing, China, **2019**. doi: 10.27493/d.cnki.gzdzy.2019.000610.
25. Lu, H.H.; Pan, L.; Han, S.H.; et al. Study on the Infrared Spectroscopy of Methyl and Chloromethyl Substituted Silatranes. Elastomer **1998**, *2*, 24–26. doi: 10.16665/j.cnki.issn1005-3174.1998.02.005.
26. Ren, H.; Zheng, Y.Y.; Wu, S. Application of Short-Wave Infrared Spectroscopy of Chlorite in Exploration of the Demingding Mo-Cu Deposit, Tibet. In Proceedings of the 9th National Conference on Metallogenic Theory and Prospecting Methods, Wuhan, China, 13–15 December **2019**; p. 444. doi: 10.26914/c.cnkihy.2019.025456.
27. Jia, R.X. Geological and Geochemical Study of the Gejiu Tin Ore Concentration Area in Yunnan Province. Ph.D. Thesis, Northwest University, Xi'an, China, **2005**.
28. Shi, R.D.; Yang, J.S.; Wang, X.B.; et al. Discovery and Significance of Rodingite in the Derni Copper Mining Area. In Proceedings of the 4th National Conference of Young Geologists, Beijing, China, 15–18 October **1999**; pp. 113–120.